Silicon-On-Insulator In-Plane Gires–Tournois Interferometers

Raphael St-Gelais, Thomas Kerrien, Hubert Camirand, Alexandre Poulin, and Yves-Alain Peter, *Senior Member, IEEE*

***Abstract*— Gires–Tournois interferometers (GTIs) based on deep-etched silicon-air Bragg mirrors and on optical quality dicing of silicon are reported. Broadband reflectivity of the deep-etched Bragg mirrors allows operation on a wavelength range exceeding the C Band window. The waveguided in-plane configuration of the devices allows interferometer lengths that are not typically achievable on chips using out-of-plane designs (e.g., L > 1 mm for a 25-GHz free spectral range). Optical characterization of GTIs having two different free spectral ranges (i.e., 25 and 100 GHz) yield off-resonance insertion losses below 2 dB and polarization-dependant losses (PDL) below 1 dB. Insertion losses and PDL are, however, more important near the resonance wavelengths, reaching, respectively, 15 and 5 dB. Calculations show that the reported devices could be useful for Michelson-GTI bandpass filters, such as optical interleavers.**

***Index Terms*— Integrated optics, interferometers, optical waveguides, silicon-on-insulator technology.**

I. Introduction

DEEP-ETCHED silicon-air Bragg reflectors were previously integrated with waveguides to form tunable in-plane Fabry–Perot cavities [1], [2]. In the current work, we investigate similar devices, in which the two silicon-air mirrors now have different reflectivities in order to form on-chip Gires–Tournois interferometers (GTIs). GTIs are mainly used for optical fiber dispersion compensation [3], [4] and in Michelson-GTI band-pass filters [5] such as optical interleavers [6]–[9]. Previous on-chip integrations of GTIs relied on out-of-plane configurations [10], [11] (optical axis perpendicular to the substrate surface). The devices presented in the current work are based on an in-plane configuration, which could be advantageous, in some contexts, compared to out-of-plane devices. For example, in this configuration, the length (L) of the interferometer is not limited, as in [10], by the thickness of the substrate. Its free spectral range (FSR) can therefore be designed with great flexibility, from a 25 GHz DWDM (dense wavelength-division multiplexing) channel spacing (L > 1 mm), to FSR > 100 nm (L < 5 μm). The waveguided in-plane configuration could also permit, through design and fabrication process modifications, monolithic integration with other on-chip components such as couplers, signal modulators, and electrical circuits for spectral tuning (e.g., thermo-optic effect, carrier injection).

Manuscript received June 13, 2012; revised August 21, 2012; accepted October 25, 2012. Date of publication November 16, 2012; date of current version November 28, 2012. This work was supported by the National Science and Engineering Research Council of Canada.

The authors are with the Department of Engineering Physics, Polytechnique Montréal, Montreal, QC H3C 3A7, Canada (e-mail: raphael.st-gelais@polymtl.ca; thomas.kerrien@enspg.inpg.fr; hubert.camirand@polymtl.ca; alexandre-2.poulin@polymtl.ca; yves-alain.peter@polymtl.ca).

Color versions of one or more of the figures in this letter are available online at http://ieeexplore.ieee.org.

Digital Object Identifier 10.1109/LPT.2012.2227142

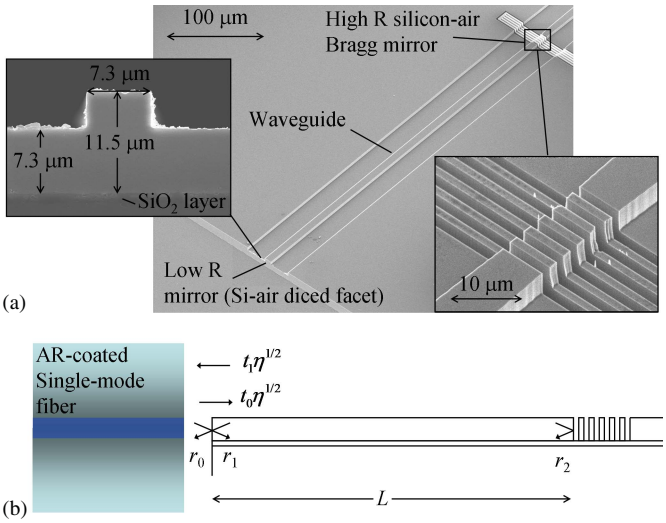

Fig. 1. (a) Scanning electron microscopy pictures and (b) schematic cross-sectional view of a silicon-on-insulator Gires–Tournois interferometer.

II. Design and Fabrication

An in-plane GTI is presented in Fig. 1. The high reflectivity mirror (at the back of the cavity) is formed by plasma etching of a 3 μm period silicon-air Bragg mirror down to the buried oxide layer of a silicon on insulator wafer (11.5 μm thick silicon device layer). The waveguide cladding is then fabricated through a second photolithography and plasma etching step. The low reflectivity mirror is finally formed by dicing the waveguide entrance facet using an ADT 7100 provectus dicing saw equipped with a small diamond grit, resinoid matrix blade (ADT Part number 00777-8003-006-QKP). A protective photoresist coating is applied prior to dicing to ensure sample cleanliness. The sawing parameters are optimized (36,500 RPM, 1 mm/s feed speed) to ensure optical surface quality and low edge chipping.

The amplitude reflection (r) and transmission (t) coefficients at each mirror are defined in Fig. 1(b). The parameter η designates the intensity coupling coefficient between the anti-reflection coated single-mode fiber (Oz optics) and the waveguide. Using this notation, the amplitude reflection coefficient of the interferometer is given by Eq. 1, where

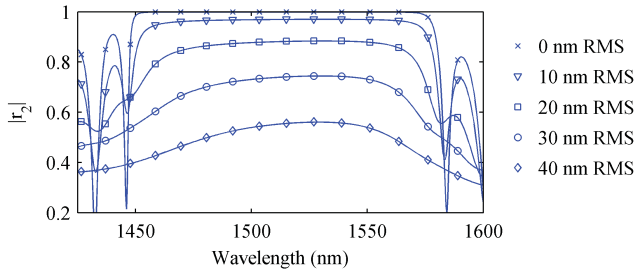

Fig. 2. Simulated amplitude reflection spectra of the Gires–Tournois back mirror (r_2), for various amounts of surface roughness at the silicon-air material interfaces. In the ideal case (no surface roughness), reflectivity exceeds 99.9% over the S and C telecommunication wavelength bands.

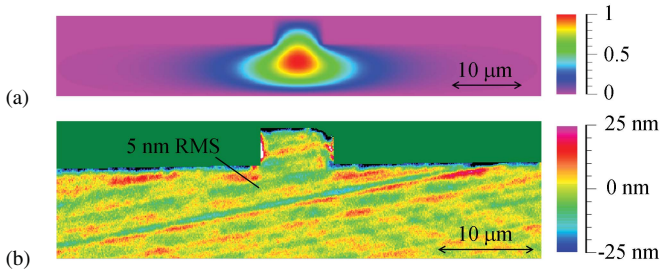

Fig. 3. (a) Simulated amplitude mode profile (arbitrary units) of the fabricated waveguide. (b) Measured roughness (5-nm RMS) of a diced silicon-air waveguide facet, which forms the low reflectivity (R = 30.6%) entrance mirror of the GTIs. The diced surface quality is significantly better than what is obtained (35-nm RMS) inside the plasma-etched silicon-air Bragg mirrors (see plasma-etched roughness profiles in [12]).

$\beta = 2\pi n_{eff}/\lambda$ and L are the propagation constant and the length of the waveguide, respectively

$$r_{GT} = r_0 + \frac{\eta t_0 t_1 r_2 e^{-2i\beta L}}{1 - r_1 r_2 e^{-2i\beta L}}. \quad (1)$$

As the waveguide cross section is relatively large, we expect the effective index to be determined essentially by silicon material dispersion, which yield $n_{eff} \approx 3.60$ at $\lambda = 1500$ nm. An imaginary part can also be added to n_{eff} to account for propagation losses. These are however found to have little influence on the calculated response and are therefore roughly approximated to a realistic 2 dB/cm value.

The nominal thicknesses of the silicon and air layers (1.5 μm each) that constitute the back mirror are as small as possible, to yield the highest possible reflection bandwidth, but are large enough to remain easily definable by contact lithography. Upon photolithography (e.g. diffraction) and plasma etching (e.g. mask undercut), the thickness of the air layers typically increases to 1.8 μm, while the silicon layers thicknesses decrease, proportionally, to 1.2 μm (i.e. the 3 μm silicon-air period is invariant). Using these dimensions, the amplitude reflection coefficient of the back mirror (r_2) is calculated with the model presented in [12]. This model accounts for losses due to Gaussian beam divergence and surface roughness at the plasma-etched material interfaces. As shown in Fig. 2, when no surface roughness is considered, the mirror is expected to yield broadband (> 100 nm) high reflectivity (> 99.9%) over the S and C telecommunication bands. However, when surface roughness is considered, the reflectivity is expected to decrease strongly, due to scattering losses.

The same model [12] can be used to predict the (r_0, r_1, t_0, t_1) coefficients of the entrance reflective facet. However, as we deal with large cross section modes, and as surface roughness on the diced facet is very low [5 nm RMS measured by white light interferometry in Fig. 3(b)], their value can be approximated as the normal incidence silicon-air Fresnel coefficients (within an error < 2%). Finally, the fiber-waveguide intensity coupling coefficient ($\eta = 0.862$) is calculated from the waveguide mode profile [Fig 3(a)], simulated using the dimensions presented in Fig. 1(a) (beam propagation method, RSoft Photonics CAD Suite).

III. Results and Discussion

Gires–Tournois interferometers having two different FSR (100 GHz and 25 GHz) were fabricated and characterized. The measurements were performed with an Agilent 86038B photonic dispersion and loss analyzer and are presented in Fig. 4, together with the simulated response obtained using Eq. 1.

Fig. 4(a) presents the measured reflectivity of a 100 GHz device over the C Band wavelength range, outlining the broadband operation of the device. In Fig. 4(b), the same device is characterized on a narrower range, showing two resonance peaks near $\lambda = 1549.7$ and $\lambda = 1550.5$ nm. The off-resonance parts of the spectrum yield interestingly low insertion losses (< 2 dB). The losses are however more important near the resonance peaks (15 dB). Fig. 4(c) presents the characterization of a longer, 25 GHz FSR, Gires–Tournois interferometer, which is found to behave similarly as the 100 GHz device. The off-resonance losses are slightly higher in this case (~2.5 dB), most likely due to the longer propagation length in the waveguide or to fabrication variations.

In Fig. 4(b), (c), the best fit between the simulations (Eq. 1) and the experimental results is obtained by reducing the fiber-waveguide coupling coefficient by 20% ($\eta = 0.7$), to account for misalignment errors, and by considering 35 nm RMS surface roughness in the plasma-etched multilayer mirror. Such amount of surface roughness is consistent with previously reported measurements of surface roughness in deep-etched trenches [12]. Using these roughness and coupling values in Eq. 1, surface roughness in the deep-etched back mirror is found to be the main source of wavelength-dependant losses. Fiber-waveguide coupling losses (η) also contribute, in a smaller extent (~3 dB), to wavelength-dependant losses, while the contribution of waveguide propagation losses is expected to be negligible (< 1 dB when considering a 2 dB/cm propagation loss coefficient).

Important reductions of the device insertion losses would therefore be achievable mainly through improvement of our etching process, rather than by design optimization. The most promising possibility would be to replace our room temperature plasma etching process by a cryogenic etching recipe. Cryogenic etching previously allowed fabrication of high finesse Fabry–Perot resonators based on deep-etched

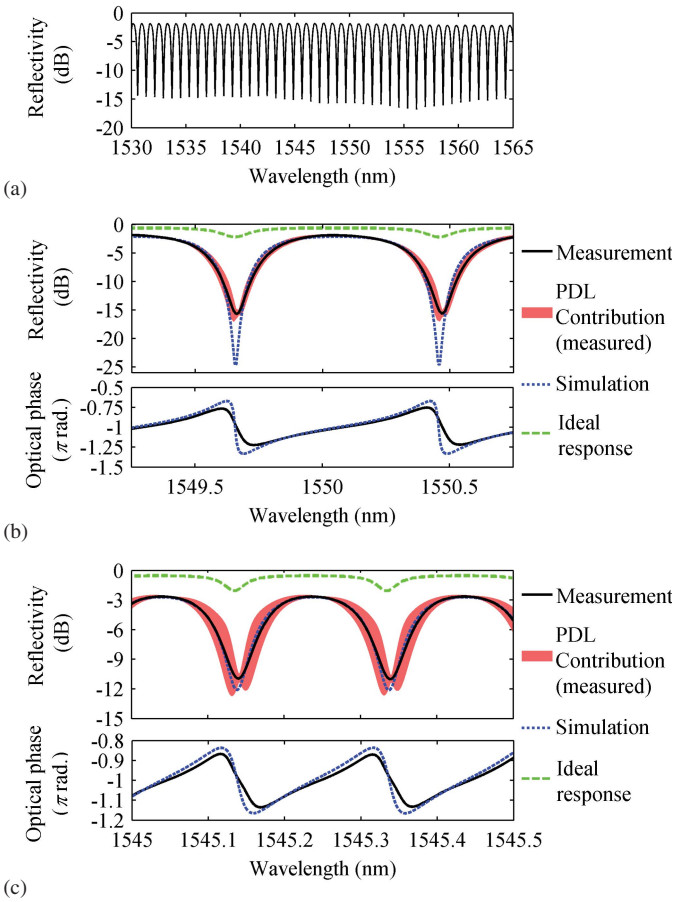

Fig. 4. (a) Measured reflectivity of a 100-GHz FSR interferometer over the C band wavelength range. (b) and (c) Measurement of the magnitude and phase response, and comparison with the theoretical model, for (b) 100- and (c) 25-GHz FSR Gires–Tournois interferometers. The PDL contribution area indicates the measured range of values for all possible polarization states.

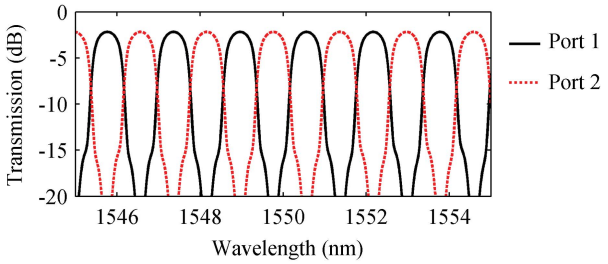

Fig. 5. Simulated interleaving capability of the reported Gires–Tournois when integrated within a Michelson interferometer. The interferometer presented in Fig. 4(b) is considered as the mirror in one arm of the Michelson, while the other arm has an R = 60% ideal mirror.

silicon-air Bragg mirrors [2], which is possible only with very low amounts of surface roughness. In the ideal case (i.e. without roughness or waveguide propagation losses, and with $\eta = 0.862$), the reflectivity of the proposed GTIs could reach −0.5 dB off-resonance with 1.5 dB wavelength-dependant losses [see the "Ideal response" traces in Fig. 4(b), (c)].

For the 100 GHz FSR device [Fig. 4(b)], polarization dependant losses (PDL) are low at off-resonance wavelengths (< 1 dB on more than 50% of each FSR). PDL however reach 5 dB near each resonance peak. The waveguide most likely has two slightly different effective indices for each of its two principal polarization axis. The resonance peak positions are therefore slightly shifted as a function of the input polarization, which cause important PDL near resonance. For the reported devices, decreasing wavelength-dependant losses would therefore also proportionally decrease PDL.

PDL is more important for the 25 GHz FSR device [Fig. 4(c)] than with the 100 GHz interferometer, most likely due to the longer waveguide that causes a larger phase shift between the two polarization axes. However, at off resonance wavelengths, PDL below 1 dB is still obtained on wavelength bands corresponding to 40% of each FSR. In Fig. 4(c), near each resonance wavelength, the PDL trace yields two clearly distinguishable resonance peaks, which allow us to determine the waveguide birefringence (Δn_{eff}). The measured value ($\Delta n_{eff} = 4.1 \times 10^{-5}$) is consistent with what is expected ($\Delta n_{eff} = 2.4 \times 10^{-5}$) from the beam propagation method simulations presented in Fig. 3(a).

As both GTIs characterized in Fig. 4 yield important signal losses (> 10 dB) and PDL (> 5 dB) at resonance, their use in optical fiber dispersion compensation devices appears unrealistic. Such device typically exploit several cascaded GTIs [3], which would each cause > 10 dB wavelength-dependant losses. Moreover, due to important signal losses, negative phase shifts occur at the resonance wavelengths [Fig. 4(b), (c)]. These negative shifts translate in a negative group delay regime that is typically unsuited for dispersion compensation.

However, the proposed interferometers could find interesting applications in Michelson-GTI (MGTI) bandpass filters such as optical interleavers. These devices typically exploit the off-resonance parts of the GTI spectrum which, in the present case, yield low insertion losses and PDL. The input mirror reflectivity ($r = 0.55$), for the reported GTIs, is also close to the value that is optimal ($r = 0.4$) for flat-top interleaving [5]. As an example, in Fig. 5, the interleaving capability of a 100 GHz FSR GTI is simulated using Eq. 1 (with the parameters that allowed the best fit with the experimental results in Fig. (4) and the formalism described in [5]. The reference mirror (in the second arm of the Michelson) is considered to have an $R = 60\%$ ideal reflectivity. Such MGTI could be implemented, as in [9], using a 50/50 optical fiber coupler and by adjusting the reference arm length with a fiber stretcher.

The simulated response of the MGTI interleaver yields 2 dB insertion losses, channel isolation in the order of 20 dB, and 50 GHz passband width (at −0.5 dB). These parameters are mostly limited by surface roughness in the deep-etched silicon-air Bragg mirror. Improving our etching process could therefore considerably improve the expected insertion losses, channel isolation, and flat-top response. Using an index matching fluid between the optical fiber and the waveguide could also improve the flat-top response by bringing the entrance mirror reflectivity closer to the ideal value ($r = 0.4$).

Tuning by thermo-optic effect or by carrier injection could compensate for drifts due to ambient temperature

variations. Electromechanical tuning was previously achieved in similar devices [13]. However, this mechanism changes the dimensions of some of the air layers inside the silicon-air Bragg mirror, which was found to induce important signal losses. Tuning by mechanisms that do not involve deformations of the Bragg mirror (e.g., thermo-optic effect, carrier injection) therefore appears preferable.

As for other waveguided planar lightwave circuit, packaging of the proposed GTIs would require high precision optical alignment (~ 1 μm tolerance). Such tight tolerance could be achieved through the integration of passive optical fiber alignment grooves. These grooves could be monolithically integrated on same wafer as the GTIs, and would be exposed to the waveguide facet through the optical quality dicing step.

IV. Conclusion

We reported what is, to our knowledge, the first in-plane implementation of a silicon-on-insulator Gires–Tournois interferometer. A simple analytical model of the device response is also proposed and is found to correspond well with the experimental results. The devices yield low loss and low PDL at off-resonance wavelengths. However, high loss and PDL were observed at resonance. These losses are caused mostly by surface roughness in the deep-etched silicon-air Bragg mirror, and could therefore be reduced by improving our plasma etching process. Without major improvements, the use of the proposed GTIs in dispersion compensating devices appears unrealistic. However, calculations show that the current devices responses could yield useful performances in Michelson-GTI bandpass filters such as optical interleavers.

References

[1] C. A. Barrios, V. R. Almeida, R. R. Panepucci, B. S. Schmidt, and M. Lipson, "Compact silicon tunable Fabry–Pérot resonator with low power consumption," *IEEE Photon. Technol. Lett.*, vol. 16, no. 2, pp. 506–508, Feb. 2004.

[2] M. W. Pruessner, T. H. Stievater, and W. S. Rabinovich, "Integrated waveguide Fabry–Pérot microcavities with silicon/air Bragg mirrors," *Opt. Lett.*, vol. 32, no. 5, pp. 533–535, 2007.

[3] D. J. Moss, *et al.*, "Tunable dispersion and dispersion slope compensators for 10 Gb/s using all-pass multicavity etalons," *IEEE Photon. Technol. Lett.*, vol. 15, no. 5, pp. 730–732, May 2003.

[4] S. Doucet, R. Slavik, and S. LaRochelle, "Tunable dispersion and dispersion slope compensator using novel Gires–Tournois Bragg grating coupled-cavities," *IEEE Photon. Technol. Lett.*, vol. 16, no. 11, pp. 2529–2531, Nov. 2004.

[5] B. B. Dingel and M. Izutsu, "Multifunction optical filter with a Michelson–Gires–Tournois interferometer for wavelength-division-multiplexed network system applications," *Opt. Lett.*, vol. 23, no. 14, pp. 1099–1101, 1998.

[6] S. Cao, C. Lin, C. Yang, E. Ning, J. Zhao, and G. Barbarossa, "Birefringent Gires–Tournois interferometer (BGTI) for DWDM interleaving," in *Proc. Opt. Fiber Commun. Conf.*, Anaheim, CA, 2002, pp. 395–396.

[7] W.-Z. Li, Q.-D. Guo, and S. Gu, "Interleaver technology review," *Proc. SPIE*, vol. 4906, pp. 73–79, Feb. 2002.

[8] H. Chao-Hsing, *et al.*, "Flat-top interleavers using two Gires–Tournois etalons as phase-dispersive mirrors in a Michelson interferometer," *IEEE Photon. Technol. Lett.*, vol. 15, no. 2, pp. 242–244, Feb. 2003.

[9] X. Shu, K. Sugden, and I. Bennion, "Novel multipassband optical filter using all-fiber Michelson–Gires–Tournois structure," *IEEE Photon. Technol. Lett.*, vol. 17, no. 2, pp. 384–386, Feb. 2005.

[10] C. K. Madsen, *et al.*, "A tunable dispersion compensating MEMS all-pass filter," *IEEE Photon. Technol. Lett.*, vol. 12, no. 6, pp. 651–653, Jun. 2000.

[11] K. Yu and O. Solgaard, "Tunable optical transversal filters based on a Gires–Tournois interferometer with MEMS phase shifters," *IEEE J. Sel. Topics Quantum Electron.*, vol. 10, no. 3, pp. 588–597, May/Jun. 2004.

[12] R. St-Gelais, A. Poulin, and Y.-A. Peter, "Advances in modeling, design, and fabrication of deep-etched multilayer resonators," *J. Lightw. Technol.*, vol. 30, no. 12, pp. 1900–1908, Jun. 15, 2012.

[13] R. St-Gelais, T. Kerrien, A. Poulin, and Y.-A. Peter, "In-plane MEMS tunable Gires–Tournois interferometers," in *Proc. CLEO/QELS*, San Jose, CA, 2010, pp. 1–2, paper CTuW2.